www.czasopisma.pan.pl PAN POLSKA AKADEMIA NAUK www.journals.pan.pl

Arch. Metall. Mater. **67** (2022), 1, 137-146

DOI: https://doi.org/10.24425/amm.2022.137482

HUAXIA ZHAO[1†], PENG GONG[2†], SHUDE JI[2*], XUE GONG[2]

ENHANCING THE STRENGTH OF Al/Mg DISSIMILAR FRICTION STIR LAP WELDED JOINT BY Zn FILLER ADDITION COMBINED WITH AN APPROPRIATE HEAT INPUT

7075-T6 Al and AZ31B Mg dissimilar alloys were friction stir lap welded with or without a Zn filler, and the effect of heat input on the joint quality was systematically studied. The experimental and finite element simulation results displayed that the formation characteristics and microstructures of the joint with or without the Zn filler were significantly affected by the heat input. The tensile shear load of joint with or without the Zn filler increased first and then decreased with the decrease of the welding speed from 200 to 50 mm/min. Moreover, the peak temperature in the stir zone was significantly decreased by the Zn filler addition, and the high temperature zone narrowed along the plate thickness direction. These changes of heat input made that longer mixing region boundary length and larger effective lap width were attained as the Zn filler was used. In addition, due to the replacement of Al-Mg intermetallic compounds (IMCs) by Al-Mg-Zn and Mg-Zn IMCs which were less harmful to the joint, the tensile shear load of the joint with the Zn filler was obviously enhanced compared to that of the joint without the Zn filler at each welding speed. The maximum tensile shear load of 7.2 kN was obtained at the welding speed of 100 mm/min.

Keywords: Friction stir lap welding; Al/Mg dissimilar alloys; Zn filler; Heat input; Tensile shear load

1. Introduction

The Al/Mg composite components have been widely used in aerospace, automatic and other manufacturing fields [1], because both of the alloys possess the characteristics of low density, high special strength and good correction resistance [2,3]. However, it is difficult for fusion welding technology to join Al/Mg dissimilar alloys. Besides porosity, inclusions and excessive deformation defects, a large amount of harmful intermetallic compounds (IMCs) are formed under a high heat input [4]. Friction stir welding (FSW) has unique advantages for joining dissimilar materials, because the welding temperature is lower than melting points of base materials (BMs) even for metal and polymer [5,6]. Therefore, the strength of FSW joint is higher compared to the joint obtained by fusion welding [7]. However, it is difficult for FSW to completely avoid the appearance of IMCs [8]. Mohammadi et al. [4] obtained Al/Mg FSW joint and found that the Al-Mg IMCs mainly formed in stir zone (SZ). Mehta et al. [9] joined Al/Mg dissimilar materials by cooling assisted FSW, and found that the cooling assistance process could reduce the amount of IMCs and then improve the joint strength. Therefore, weakening the harmful effect of IMCs is meaningful to improve the strength of the FSW joint of Al/Mg dissimilar materials.

A third material as an interlayer has been employed to control the formation of IMCs during welding process. For fusion welding, pure Zn, Ti, Fe, Sn, Ni, and other binary or ternary alloys are the main filler materials [10]. These filler materials are beneficial to improving the microstructure and tensile strength of the joints. For FSW process, Zn is popularly used as the filler material [11-13]. Niu et al. [11] joined AZ31B Mg and 7075-T6 Al alloys with a pure Zn interlayer by friction stir lap welding (FSLW), and obtained a wider SZ, a larger effective lap width (ELW) and a higher shear strength compared with the joint without Zn interlayer. Farahain et al. [12] employed pure Mg and Al as BMs to carry out FSLW with a Zn filler. They found that Al-Mg IMCs were replaced by Mg-Zn and Al-Mg-Zn IMCs, and the shear strength of the pure Al/Mg lap joint was improved 25% compared to the joint without Zn. Gan et al. [13] performed friction stir induced brazing to join Al/Mg dissimilar materials with a Zn filler. Their results showed that the formation of Al-Mg IMCs could be effectively blocked under an appropriate welding

[1] AVIC MANUFACTURING TECHNOLOGY INSTITUTE, BEIJING 100024, P. R. CHINA
[2] SHENYANG AEROSPACE UNIVERSITY, COLLEGE OF AEROSPACE ENGINEERING, SHENYANG 110136, P. R. CHINA

* Corresponding author: superjsd@163.com

† Peng Gong and Huaxia Zhao contributed equally to this work

parameter, but Al-Mg IMCs formed when the heat input induced by a large rotating velocity was too high. During the friction stir brazing process, the rotating tool only stirs in the upper sheet, in which the flow ability of materials along the thickness direction is weakened, resulting in a relatively small joint strength. When the rotating pin plunges into the lower sheet, the material flow along the thickness direction is improved, and the mechanical interlocking between the upper and lower sheets is enhanced. Therefore, when the Zn filler is used as an interlayer, the FSLW with the rotating pin plunging into the lower plate has a larger research value compared to friction stir induced brazing.

In fact, a relatively high heat input is conducive to improving the flow ability of material in the SZ, while it would lead to more hard and brittle IMCs for the Al/Mg dissimilar FSLW joint [14]. The effect of heat input on the microstructure and mechanical properties of FSLW joint with the Zn filler should be further researched. In this work, the effect of heat input was studied by varying welding speed, and welding temperature in the SZ was revealed by experimental measurement and numerical simulation.

2. Experimental produces and finite element modeling

FSLW was employed to join AZ31B Mg and 7075-T6 Al alloys. The dimensions of BMs were 180 mm×150 mm×3 mm. AZ31B Mg alloy was set as the upper plate during welding process, and the lap width was 50 mm. Pure Zn foil as the filler has a dimension of 150 mm×50 mm×0.1 mm. Before welding, the BMs were polished by sand papers and washed by acetone. The welding process diagram is stated in Fig. 1. The welding direction was perpendicular to the rolling direction of the BMs, and the materials at retreating side (RS) bore external load during tensile shear test. H13 steel was the material of rotating tool. The profile of the shoulder with a diameter of 13 mm was concentric-circle-flute, which was conductive to enhancing the flow behavior of materials under the shoulder. The diameters of rotating pin bottom and tip were 6 mm and 4 mm, respectively, and the pin length was 3.7 mm. The rotating pin with right-screwed thread rotated counterclockwise during welding to reduce material spillage, thus avoiding excessive thinning of the weld [15]. The rotating velocity was kept in 1200 rpm, and the welding speed was varied from 50 mm/min to 200 mm/min with an increment of 50 mm/min. The rotating shoulder plunged 0.2 mm into the upper plate. K-type thermal couples were used to measure the temperature history. Point A was the measuring position, where was 7 mm away from the welding center line and 3 mm lower than the top surface of upper plate.

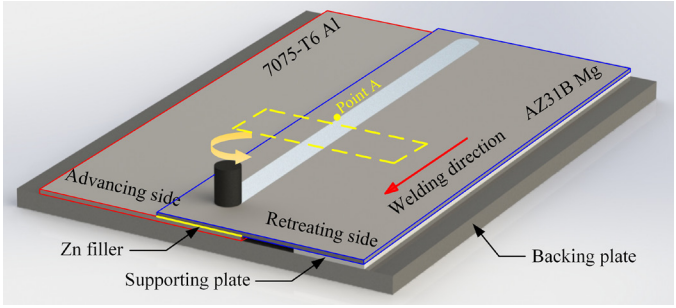

Fig. 1. Schematic of dissimilar Al/Mg FSLW with a Zn filler

The specimens of metallographic and mechanical properties were cut perpendicular to the welding direction. After polished, the metallographic specimens were etched 18 s by the etching solution (5 ml acetic acid, 4.2 g picric acid, 10 ml distilled water and 100 ml ethanol). Cross section was observed by an optical microscope (OM, OLYMPUS GX71). Microstructures and elements distribution were revealed by a scanning electron microscope (SEM, VEGATE-Scan) equipped with an energy dispersion spectrography (EDS). The tensile shear specimen was taken at the stable stage of the weld, in which the heat input and microstructure were relatively uniform, and its position is shown as the yellow dotted box in Fig. 1. The width of tensile shear specimen was 30 mm, and three specimens for each welding condition were prepared. The tensile shear test was performed by a universal testing machine (MTS Model E45.106) at a displacement rate of 3 mm/min at room temperature. The fracture morphologies were observed by the OM and SEM.

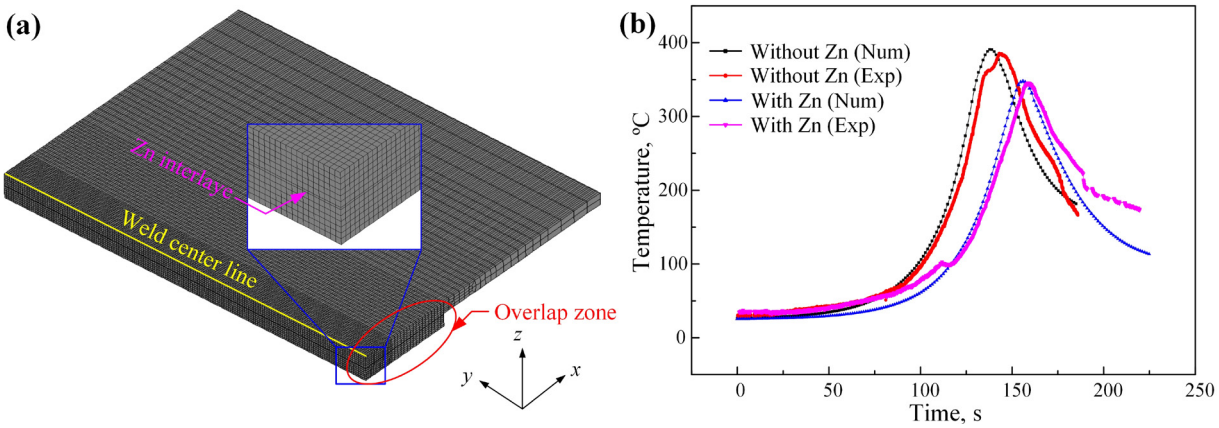

Fig. 2. FEA model verification: (a) mesh generation and (b) comparisons of thermal cycles of point A between the simulation and experimental results at welding speed of 50 mm/min

Finite element analysis (FEA) method was used to reveal the temperature distribution during the welding process. MSC. Marc software was used, and the size of the model was similar with the BMs in experiment. The size of the mesh near the weld was set as 0.5 mm, and a larger mesh size was selected far away from the weld center (Fig. 2a). The mesh type was eight-node hexahedron element. The contact heat transfer and the heat convection coefficient were 200 W/m^2·°C and 40 W/m^2·°C, respectively. The heat input was mainly produced by friction between BMs and rotating tool [16]. The heat produced by the shoulder could be expressed as:

$$q_1 = \frac{2}{3}\pi\mu\omega p \cdot \left(R_1^3 - R_2^3\right) \tag{1}$$

Where q_1 and μ were the friction heat power and the friction coefficient between the shoulder and the BMs, respectively; ω was the angular velocity of the rotating tool; p was the vertical force exerted by the shoulder on the BMs; R_1 and R_2 were the radiuses of the shoulder and the rotating pin bottom.

The heat produced by the side surface of rotating pin could be expressed as:

$$q_2 = \frac{2\pi\mu\omega p}{3\sin\alpha} \cdot \left(R_2^3 - R_3^3\right) \tag{2}$$

Where q_2 was the friction heat power between the pin side surface and the BMs; R_3 was the radius of pin tip; α was the half conical angle of rotating tool.

The heat produced by the tip surface of rotating pin could be expressed as:

$$q_3 = \frac{2}{3}\pi\mu\omega p R_3^3 \tag{3}$$

Where q_3 was the friction heat power between the pin tip surface and the BMs.

The densities of AZ31B Mg alloy and 7075 Al alloy were 2770 kg·m^{-3} and 1790 kg·m^{-3}, respectively. The values of specific heat capacity and thermal conductivity of AZ31B Mg and 7075 Al alloys were the same as those in literatures [16] and [17].

The thermal cycle curves on point A during numerical simulation and experimental process are displayed in Fig. 2b. For the experimental process, the peak temperature was reduced by 38ºC at the welding speed of 50 mm/min as a Zn filler was used. The simulated thermal cycle for the welding processes with or without the Zn filler was in good agreement with the experimental result, presenting a trend of rapid increase in the heating stage and then sharp decrease in the cooling stage. The maximum deviation of peak temperatures between simulation and experimental results was 2.3% for the welding process without Zn filler, and this deviation was 1.7% for the process with Zn filler. These deviations could be acceptable, which proved that the finite element model in this study was reasonable.

3. Results

3.1. Joint formation

The joint formation is significantly affected by heat input during welding process [18]. As mentioned above, the peak temperature can be reduced by the addition of Zn filler (Fig. 2b). The formation characteristics of the joints with or without Zn filler at different welding speeds are analyzed to study the combination effects of the heat input and the Zn filler addition (Figs. 3 and 4).

For the joints without the Zn filler, the lap interface adjacent to the SZ bends toward the top surface of the joint due to the material flow behavior when the length of the rotating pin is longer than the thickness of upper plate [19]. A hook and a cold lap are formed at advancing side (AS) and RS, respectively, as shown in Fig. 3a. Compared with the hook upward bending only, the cold lap always extends into the SZ, leading to a small ELW. A distinct mixing region (MR) of Al and Mg substrates exists between the hook and the cold lap, which is almost entirely located at the SZ bottom (Fig. 3). Broadening joining interface and achieving a strong interface is important for FSLW [20].

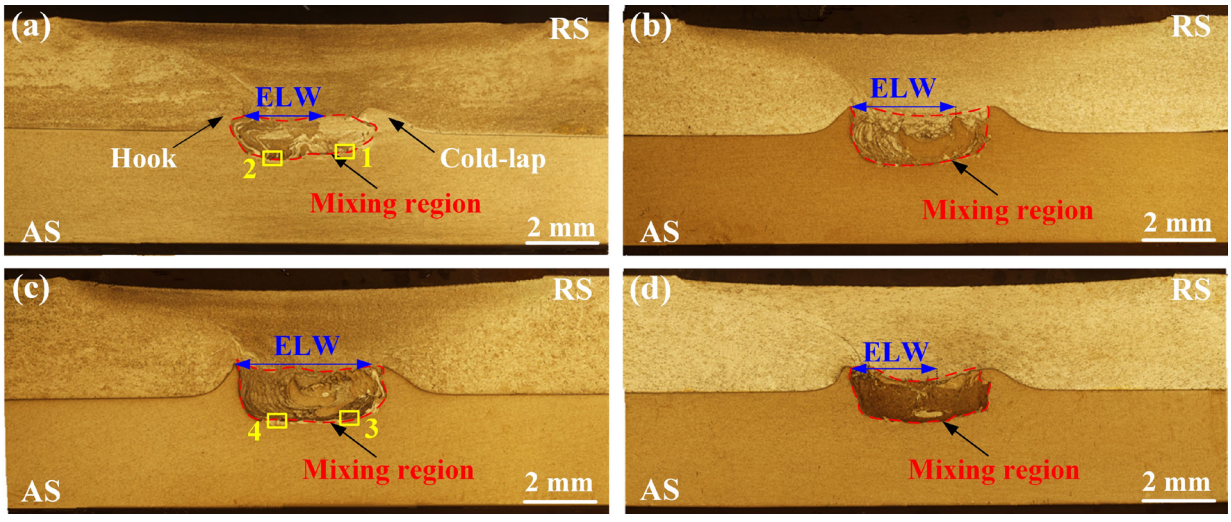

Fig. 3. Macrostructures of dissimilar Al/Mg FSLW joints at different welding speeds: (a), (b), (c) and (d) 200, 150, 100 and 50 mm/min

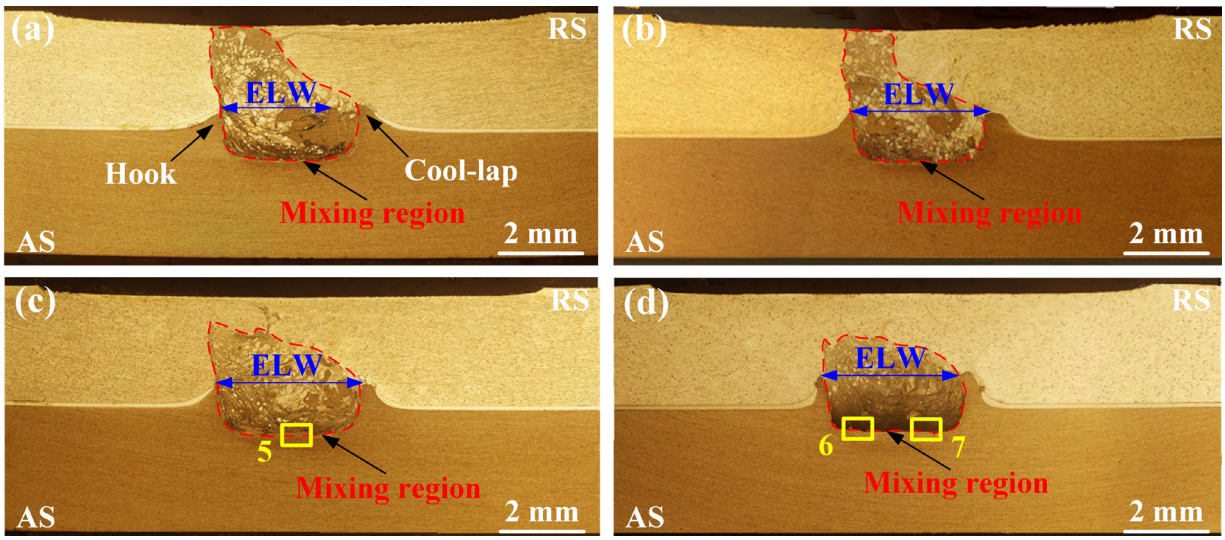

Fig. 4. Macrostructures of dissimilar Al/Mg FSLW joints with Zn filler at different welding speeds: (a), (b), (c) and (d) 200, 150, 100 and 50 mm/min

Therefore, the ELW and the boundary length of the MR in the lower plate are significant indexes for evaluating the formation of lap joint [21]. There are differences in the joint formation when different welding speeds are employed. The ELW and the MR boundary of the joint at the welding speed of 200 mm/min are both the smallest (Fig. 5). Although the mechanical interlocking is formed, it is weak because the Al substrate with a large size is continuously distributed in the MR and adjacent to the cold lap at the RS. It can be deduced that the heat input at the welding speed of 200 mm/min is not enough to induce sufficient plasticization of materials in the SZ, and the time of mechanical agitation induced by the rotating tool for the materials per unit length along the welding direction is too short. Therefore, the flow ability of materials is poor, which is the reason for the unsatisfactory formation of the joint in Fig. 3a. Generally, the heat input can be simply characterized by the heat index (*HI*), which is expressed as follows [22]:

$$HI = 10^{-4}\omega^2/v \tag{4}$$

Where ω and v represent rotating velocity and welding speed, respectively. The heat input is proportional to ω^2/v, which means that the heat input is increased with decreasing the welding speed. The flow stress of the material in the MR is reduced when the welding speed is decreased, and the Al substrate in the MR at the RS is gradually separated from the cold lap (Fig. 3b and c). Therefore, the ELW and the MR boundary are both increased with decreasing the welding speed, and the maximum values are obtained when the welding speed of 100 mm/min is employed (Fig. 5). The mechanical interlocking at the SZ bottom is also improved by the greater flow ability of materials. Moreover, when the welding speed is further reduced to 50 mm/min, although the size of the Al substrate in the MR is smaller due to the larger material flow rate, the MR size is relatively small. This result is mainly because the pushing force induced by the materials with a near liquid state in the MR to the materials in the thermo-mechanically affected zone (TMAZ) is reduced.

The joint formation is significantly improved by the addition of Zn filler, as shown in Fig. 4. The ELW presents a similar evolution trend to that of the joints without Zn filler, and the maximum value is obtained at the welding speed of 100 mm/min (Fig. 5). Compared with the joint without the Zn filler, the size

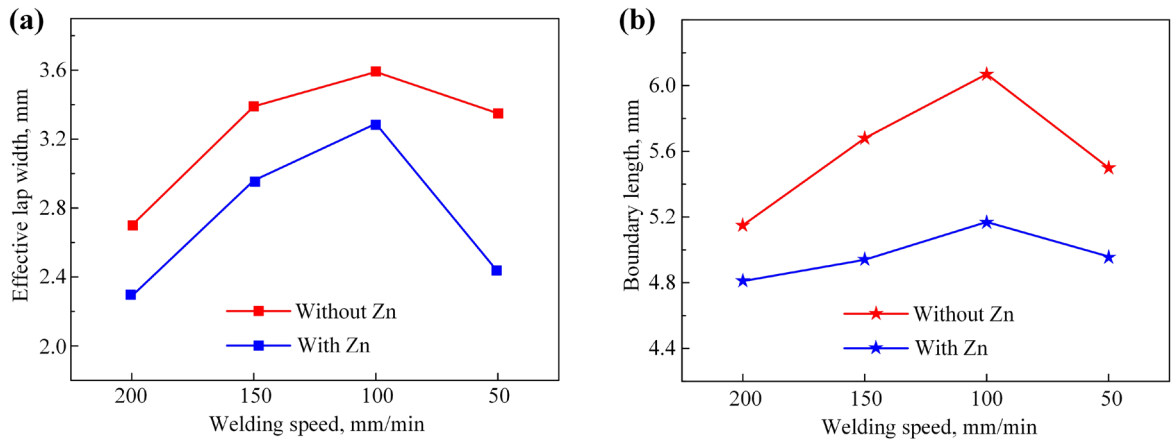

Fig. 5. Formation characteristics of different joints: (a) ELW and (b) boundary length of the MR in the lower plate

of the cold lap at the RS is significantly decreased by the Zn addition, which shows a similar morphology with the hook at the AS when the welding speeds of 150, 100 and 50 mm/min are used. For the joint without Zn filler, the Al substrate with a large bulk morphology still exists at the RS of the MR even under a relatively high heat input at the welding speed of 100 mm/min. However, the Al substrate at the RS of the joint with Zn filler at the welding speed of 150 mm/min is completely broken, which indicates a great flow ability of materials although the heat input is relatively small at this welding speed. It can be inferred that this difference in joint formation is related to the addition of Zn filler. The temperature cycle curves in the center of the weld at different welding speeds are obtained by the FEA, as displayed in Fig. 6. The peak temperatures in the center of the weld with Zn filler are all lower than those without Zn filler. It can be visualized that molten Zn, whose molten point is 419.5°C [23], is wrapped on the surface of the rotating pin in a liquid state, reducing the friction heat produced between the pin and the materials in the SZ. Therefore, the peak temperature in the weld center is decreased by the Zn addition. In addition to the peak temperature at the weld center, the simulated temperature filed distribution also changes significantly by the Zn filler, as displayed in Fig. 7. The high temperature zone of the joint with Zn filler (Fig. 7a) is obviously smaller than that of the joint without Zn filler (Fig. 7b). The temperature distributions under two processes along the thickness direction are shown in Fig. 7c and d. The heat input in the TMAZ below the SZ of the joint with Zn addition is relatively small compared with that of the joint without Zn filler.

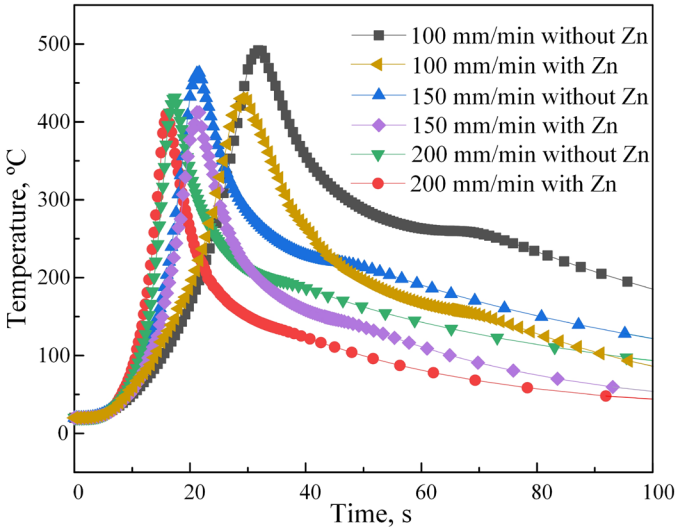

Fig. 6. Peak temperatures at the weld center obtained by finite element analysis

The formation characteristics of the joint are related to the heat input. The MRs in the joints with Zn filler in Fig. 4a and b extend to the upper surface of the weld. The height of the MR is gradually decreased with the decrease of the welding speed (Fig. 4c and d). It can be attributed to the difference in the material flow ability at different heat inputs. For the welding process at 200 mm/min, the ratio of rotating velocity to welding speed is small and the plasticization degree of the materials is low, making that a smaller amount of materials under the shoulder are transferred from the AS to the RS with the rotation of rotating tool. With decreasing the welding speed, the materials cumulated at the RS under the shoulder are increased gradually due to the larger ratio of rotating velocity to welding speed, producing a large extrusion force to the MR materials with a low deformation resistance because of more liquid Zn. On the other hand, the materials containing liquid Zn adjacent to the rotating pin transferred down into the SZ bottom are increased per unit time. Therefore, the MR in the SZ upper part

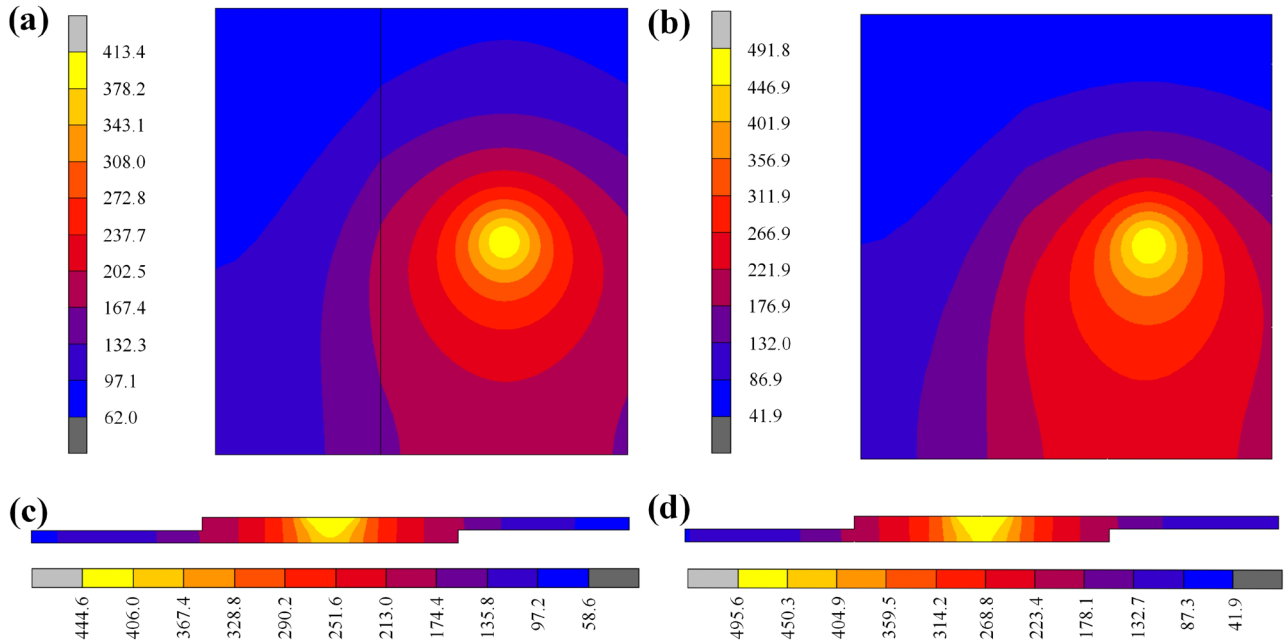

Fig. 7. Temperature field distributions by FEA at the welding speed of 100 mm/min: upper surface of (a) joint with Zn and (b) joint without Zn; cross-section of (c) joint with Zn and (d) joint without Zn

is narrowed in Fig. 4b, and eventually separated from the upper surface of the weld (Fig. 4c and d). Moreover, the ELW and the MR boundary in the lower plate of the joint with the Zn filler present a similar change to those without Zn addition with the decrease of the welding speed. The largest ELW and the MR boundary are obtained at the welding speed of 100 mm/min (Fig. 5). The ELW and the MR boundary in Fig. 4 are both greater than those in Fig. 3 at the same welding speed because the flow ability of materials in the SZ is promoted by the Zn filler. It can be concluded that the formation of the lap joint of 7075-T6 and AZ31B dissimilar alloys is significantly affected by the heat input and the Zn filler.

3.2. Microstructure

Microstructure is one of the key factors that significantly affect the strength of the FSW joint [24]. The microstructure morphologies of the joints without Zn filler at different welding speeds are presented in Fig. 8. For the joint at 200 mm/min, the main part in the MR bottom is black gray Mg substrate, on which the light gray Al strips with a large size are continuously distributed (Fig. 8a). Some flocculent structures with a similar color to the Al strip exist at the interface between the Al strip and the Mg substrate, as displayed in the enlarged view of Fig. 8a. It can be inferred that these flocculent structures are $Al_{12}Mg_{17}$ which is one of the typical Al-Mg IMCs, according to the reported results [25]. A large amount of $Al_{12}Mg_{17}$ can be found near the MR boundary at the AS (Fig. 8b). The prerequisite for the formation of Al-Mg IMCs is the presence of the liquid phase. In theory, the peak temperature of the weld center during FSLW at the welding speed of 200 mm/min (Fig. 6) is lower than the melting points of 7075-T6 (475~635ºC) and AZ31B (650ºC) alloys [26,27]. For the joint in Fig. 3a, the formation of liquid phase can be attributed to the drastic atomic diffusion behavior under the rotation effect of the rotating tool as well as the heat input. This inference can be supported by Yang et al. [28]. The peak temperature in the weld center at 200 mm/min (Fig. 6) is close to the eutectic temperature of 437°C, and the product corresponding to this condition is $Al_{12}Mg_{17}$ based on the Al-Mg binary phase diagram [29]. This can explain why there is a large number of flocculent $Al_{12}Mg_{17}$ in the MR at 200 mm/min.

The microstructure changes significantly when the welding speed drops to 100 mm/min. The enlarged view of region 3 marked in Fig. 3c displays that the concentrated flocculent $Al_{12}Mg_{17}$+Mg still exists at the RS of the MR where is rich in Mg element (Fig. 8c). It is noteworthy that the continuous flocculent $Al_{12}Mg_{17}$+Mg is basically separated from the MR boundary, which is different with that in Fig. 8a and b. Compared with the microstructure in Fig. 8b, the concentrated flocculent $Al_{12}Mg_{17}$+Mg adjacent to the MR boundary at the AS is replaced by the banded structures with a certain trend, as presented in Fig. 8d. According to the reported results [30], the structure with the above morphological characteristic can be determined as Al_3Mg_2+Al. The XRD pattern of the structures near the MR boundary of the joint at 100 mm/min confirms that Al_3Mg_2 is formed in the MR bottom besides $Al_{12}Mg_{17}$ (Fig. 8e). Combined with the simulation results in Figs. 6 and 7, the peak temperature in the weld center of the joint without Zn filler at 100 mm/min is higher than the Al-Mg eutectic temperature of 450°C. Therefore, the Al_3Mg_2 is produced preferentially at the MR boundary where is rich in Al element under the relatively high heat input at the welding speed of 100 mm/min.

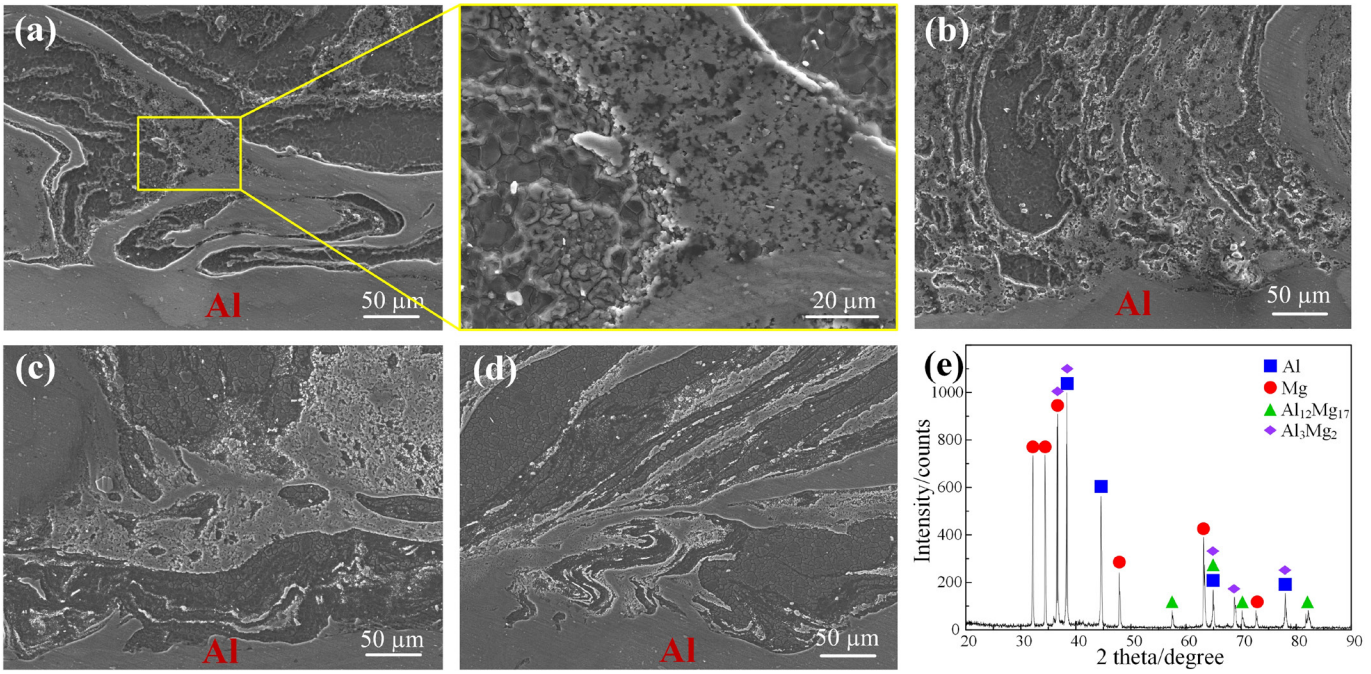

Fig. 8. The microstructures in the regions at the joints without Zn filler: (a) 1 and (b) 2 marked in Fig. 3a; (c) 3 and (d) 4 marked in Fig. 3c; (e) XRD pattern on the MR bottom at 100 mm/min

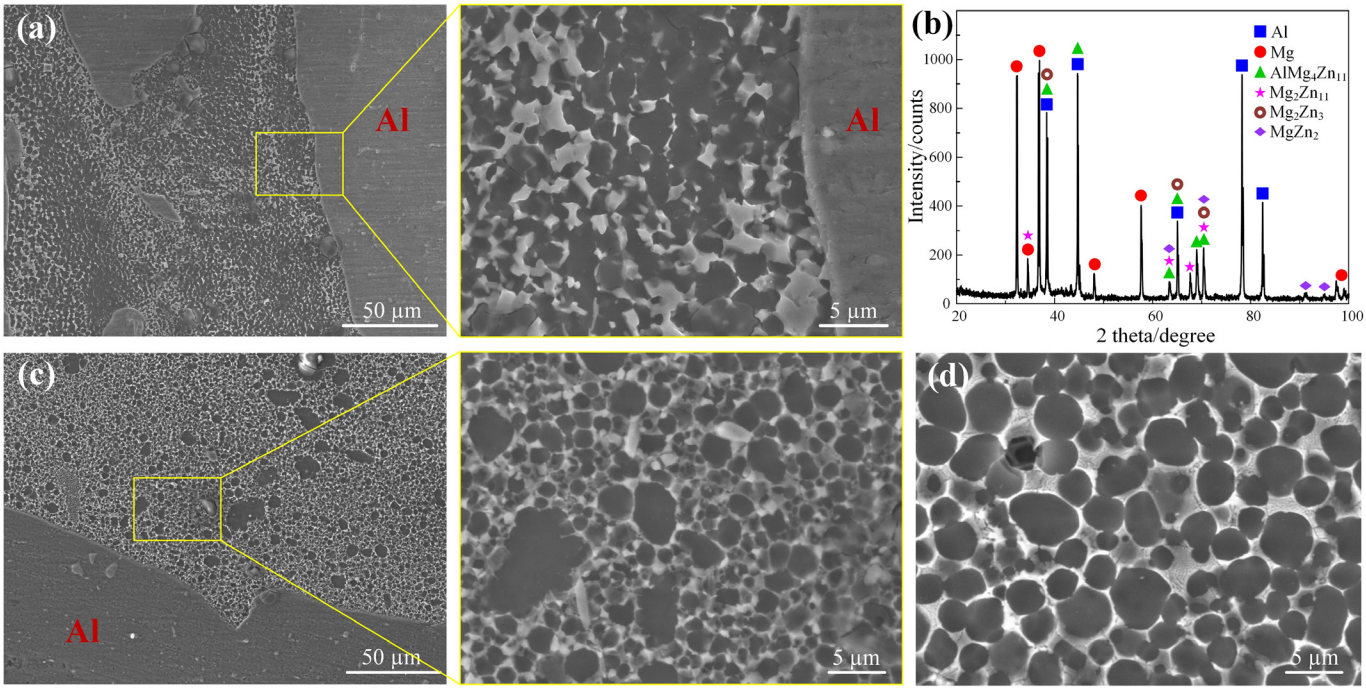

Fig. 9. The microstructures in the regions at the joints with Zn filler: (a) 5 marked in Fig. 4c; (b) XRD pattern on MR bottom at 100 mm/min; (c) 6 and (d) 7 marked in Fig. 4d

Compared with the FSLW joints of Al and Mg dissimilar alloys without Zn filler, the microstructure of the joints with Zn addition presents remarkable difference, as displayed in Fig. 9. The continuous flocculent or banded structures concentrated at the MR bottom do not appear. Instead, white particles with a small size of 1~2 μm are evenly distributed in the MR (Fig. 9a). The enlarged view of the boundary between the Al and Mg substrates states that these discontinuous particles are mainly separated from the Al substrate at the MR boundary. The XRD pattern in Fig. 9b reveals that these uniform particles are Al-Mg-Zn and Mg-Zn IMCs, and no Al-Mg IMCs are detected in the MR of the joint with Zn addition. It is noteworthy that the simulated peak temperature of the joint with Zn addition at 100 mm/min is 444.6°C, which exceeds the eutectic temperature of 437°C corresponding to $Al_{12}Mg_{17}$ and is close to the eutectic temperature of Al_3Mg_2 (450ºC). It can be inferred that the inhibition of the formation of Al-Mg IMCs is related to the addition of the Zn filler. Gan et al. [13] reported that the eutectic reaction of L→Mg-Zn+Al-Mg-Zn occurred at the temperature of 340°C, which is much lower than the temperature of Al-Mg eutectic reaction. Moreover, Mg possesses the same lattice structure of close-packed hexagonal as Zn, while the lattice structure of Al is face-centered cubic lattice. Therefore, Mg-Zn and Al-Mg-Zn IMCs are preferentially formed under the conditions of relatively low heat input and sufficient Zn content in the MR. When the welding speed drops to 50 mm/min, Zn accumulated at the MR bottom increases significantly due to the increase of the mixed materials transferred downward with the rotation of the rotating pin per unit time. This can correspond to the morphology of the MR in Fig. 4d. Therefore, the morphology of the IMCs particles in Fig. 9c and d represents difference compared with that at 100 mm/min. The number and size of IMCs are significantly increased, thereby possessing a tendency to grow into a continuous network structure under the relatively high heat input.

3.3. Mechanical property

The joint formation and microstructure are decisive factors for the mechanical property of the FSW joint [31]. The tensile shear test is carried out to investigate the influence of the heat input and the Zn filler on the mechanical property of dissimilar Al and Mg FSLW joint, and the results are displayed in Fig. 10. The tensile shear loads of the joints with and without Zn filler both increase first and then decrease with decreasing the weld-

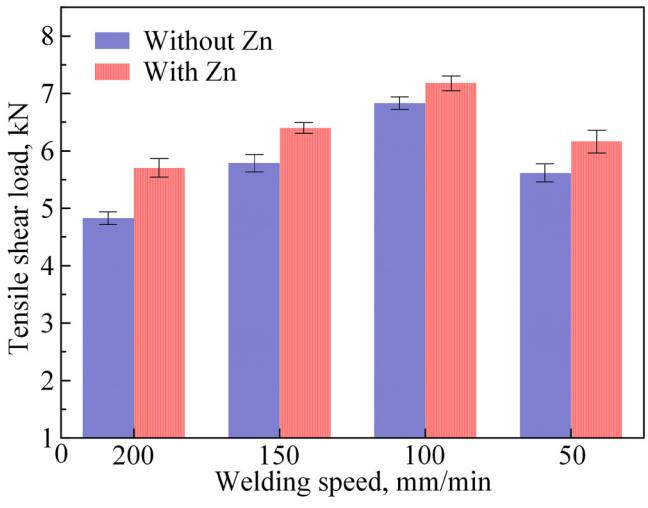

Fig. 10. Tensile shear load of dissimilar Al/Mg FSLW joints

ing speed, and the maximum values are both obtained at the welding speed of 100 mm/min. This trend is closely related to the evolution of joint formation and microstructure which are greatly influenced by the heat input. For the joints with and without the Zn filler, both the ELW and the MR boundary length achieve the maximum at the welding speed of 100 mm/min, and the IMCs exist in the MR with relatively good morphological characteristics. It is worth noting that the tensile shear load of the joint with Zn addition is evidently higher than that of the joint without Zn filler no matter which welding speed is used, and the largest load is 7.2 kN. The maximum load difference between the joints with and without Zn filler appears when the welding speed of 200 mm/min is used, and the load is increased by 17.5% by Zn addition. This phenomenon is attributed to the huge difference of the MR formation and the IMCs morphology between these two joints.

The fracture locations of the joints with and without Zn filler are shown in Fig. 11. There are two typical fracture paths existing in all joints: the path 1 that starts from the hook at the AS and then propagates along the MR boundary in the lower plate; the path 2 that starts from the cold lap at the RS. The extension direction of path 2 depends on the morphology of cold lap. As the cold lap has a small size, the failure crack tends to propagate through the upper plate to the top surface of the weld, which means a tensile fracture (Fig. 11a, c, and d). The crack propagates into the SZ when the cold lap extends into the SZ, indicating a shear fracture (Fig. 11b). In terms of joint formation characteristics, MR boundary length and ELW are significant factors affecting the shear strength of the joint, which correspond to path 1 and 2, respectively. For the joints without Zn filler, the MR boundary length in the lower plate at 100 mm/min is obviously longer than that at 50 mm/min, and the

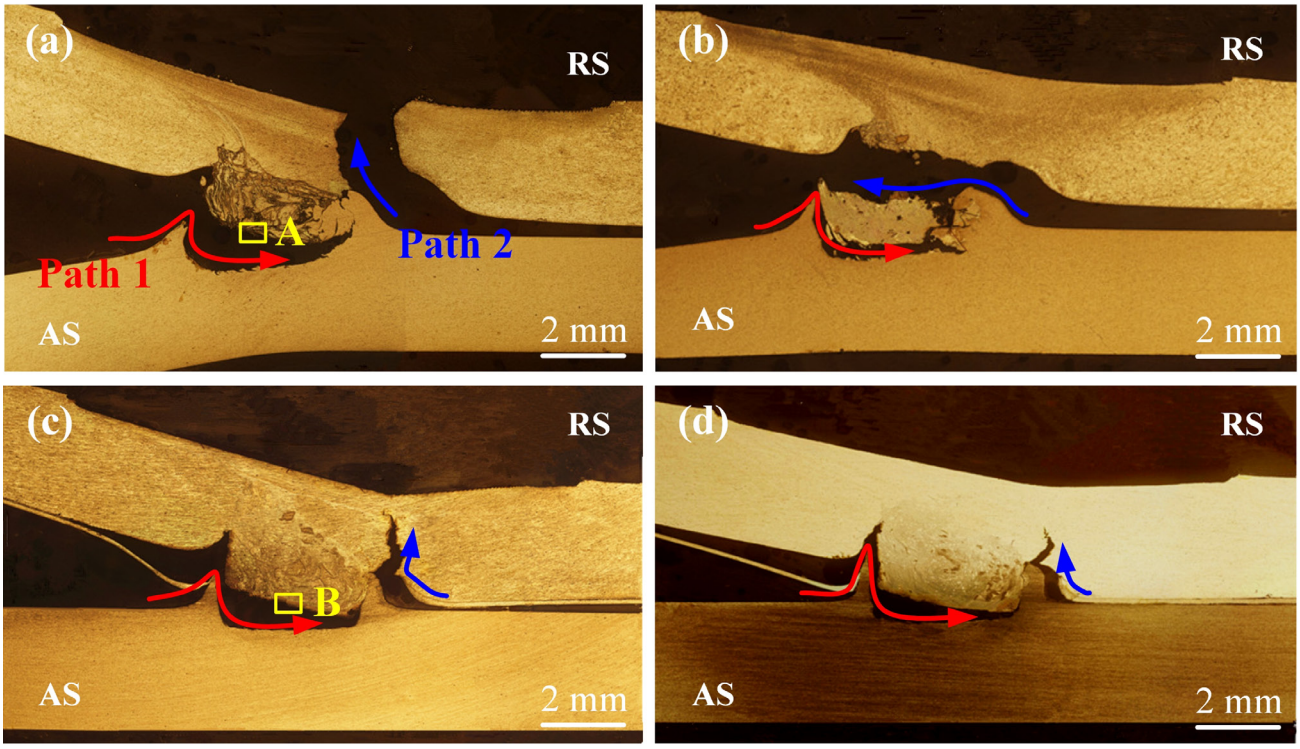

Fig. 11. Fracture locations in different joints: (a) and (b) joints without Zn filler at 100 and 50 mm/min; (c) and (d) joints with Zn filler at 100 and 50 mm/min

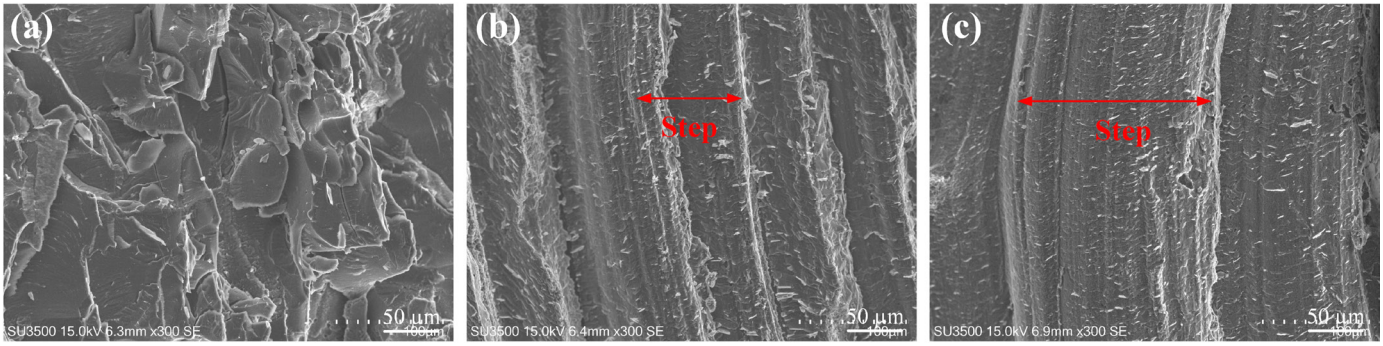

Fig. 12. Enlarged views of fracture surfaces: (a) region A marked in Fig. 11a; (b) region B marked in Fig. 11c and (c) the similar location to region B in the joint at 200 mm/min

ELW at 50 mm/min is the smallest due to the cold lap extending into the SZ (Fig. 5). Moreover, the fracture of the joint without Zn filler displays obvious brittle fracture, and large cracks exist on the fracture surface (Fig. 12a), which is related to the hard and brittle Al-Mg IMCs with the continuous morphology. It can be inferred that the size of Al-Mg IMCs near the MR boundary at 50 mm/min is larger than that at 100 mm/min because of the relatively high heat input. Therefore, the maximum tensile shear load of 6.8 kN at 100 mm/min is 1.2 kN larger than that at 50 mm/min.

When the Zn filler is used, the MR boundary and ELW both conspicuously increased due to the improvement of the material flow ability. On the other hand, the continuous Al-Mg IMCs adjacent to the MR boundary are replaced by the fine Al-Mg-Zn and Mg-Zn IMCs particles. The hardness and brittleness of Al-Mg-Zn and Mg-Zn IMCs are smaller than those of the Al-Mg IMCs according to previous studies [32]. The above-mentioned improvement of the joint formation and microstructure is conducive to extending the propagation path of the failure crack and retarding its propagation rate. These are why the strength of joint with Zn addition is increased compared with that of the joint without Zn filler. The fracture morphologies of the joints with Zn addition in Fig. 12b and c indicate that the step length of the joint at 200 mm/min is much longer than that at 100 mm/min. Although the IMCs adjacent to the MR boundary possess smaller size, the tensile shear load of this joint is lower because of the small and smooth MR boundary. The highest tensile shear load of the joint with Zn filler at 100 mm/min can be attributed to the largest MR boundary length and ELW and the discontinuous Al-Mg-Zn and Mg-Zn IMCs particles with an appropriate size.

4. Conclusions

The effect of the heat input on the macrostructure, microstructure and tensile shear strength of the dissimilar 7075-T6 Al/AZ31B Mg FSLW joint with or without Zn filler was systematically analyzed according to experimental and simulation results. The following conclusions can be drawn.

(1) The peak temperatures in the stir zone of the joints with and without Zn filler were both increased with decreasing the welding speed from 200 to 50 mm/min. Under the effect of the change of heat input, the boundary length of mixing region of Al and Mg and the effective lap width of these two joints were both increased first and then decreased, and the maximum values were both obtained at the welding speed of 100 mm/min. The morphology and distribution of IMCs were improved due to the suitable heat input when the welding speed dropped to 100 mm/min. These results made that the tensile shear strength of both joints reached the optimum value at the welding speed of 100 mm/min.

(2) The peak temperature was obviously reduced as the Zn filler was used compared to the joint without Zn filler, which could be attributed to the liquid state of Zn during welding process. Although the heat input was decreased by the Zn filler, the joint formation was significantly improved with larger mixing zone boundary length and effective lap width. Moreover, the fine Al-Mg-Zn and Mg-Zn IMCs particles replaced the continuous Al-Mg IMCs formed in the joint without Zn filler. Therefore, the tensile shear load of the joint was increased by Zn filler addition, and the largest load of 7.2 kN was attained at 100 mm/min.

Acknowledgement

This work is supported by the National Natural Science Foundation of China (No.51874201).

REFERENCE

[1] Y. Wang, G. Luo, J. Zhang, Q. Shen, L. Zhang, Mat. Sci. Eng. A **559**, 868-874 (2013).
[2] M. Balamagendiravarman, S. Kundu, S. Chatterjee, Arch. Metall. Mater. **62** (3), 1813-1817 (2017).
[3] W.S. Chang, S.R. Rajesh, C.K. Chun, H.J. Kim, J. Mater. Sci. Technol. **27**, 199-204 (2011).
[4] J. Mohammadi, Y. Behnamian, A. Mostafaei, H. Izadi, T. Saeid, A.H. Kokabi, A.P. Gerlich, Mater. Charact. **101**, 189-207 (2015).
[5] Y. Huang, X. Meng, Y. Xie, J. Li, L. Wan, Compos. Part B-Eng. **163** (15), 217-223 (2019).
[6] Y. Huang, X. Meng, Y. Wang, Y. Xie, L. Zhou, J. Mater. Process. Technol. **257**, 148-154 (2018).
[7] W.F. Xu, X.K. Wu, J. Ma, H.J. Lu, Y.X. Luo, J. Mater. Res. Technol. **8**, 6029-6040 (2019).
[8] F. Liu, Z. Zhang, L. Liu, Mater. Charact. **69**, 84-89 (2012).
[9] K.P. Mehta, P. Carlone, A. Astarita, F. Scherillo, F. Rubino, P. Vora, Mat. Sci. Eng. A **759**, 252-261 (2019).
[10] L. Liu, D Ren, F. Liu, Materials **7**, 3735-3757 (2014).
[11] S. Niu, S. Ji, D. Yan, X. Meng, X. Xiong, J. Mater. Process. Technol. **263**, 82-90 (2019).
[12] M. Farahani, M. Divandari, Int. J. Syst. Signal. Control. Eng. Appl. **9**, 86-96 (2016).
[13] R. Gan, Y. Jin, Sci. Technol. Weld. Joining **23**, 164-171 (2018).
[14] S. Ji, Z. Li, Z. Zhou, B. Wu, J. Mater. Eng. Perform. **26**, 5085-5096 (2017).
[15] M. Guan, Y. Wang, Y. Huang, X. Liu, X. Meng, Y. Xie, J. Li, Mater. Lett. **255**, 126506 (2019).
[16] J. Tang, Y. Shen, J. Alloy Compd. **666**, 493-500 (2016).
[17] C. Zhang, G. Ma, J. Nie, J. Ye, Int. J. Adv. Manuf. Technol. **78** (5-8), 1259-1264 (2015).
[18] B. He, L. Cui, D.P. Wang, H.J. Li, C.X. Liu, Acta Metall. Sin-Engl. **33**, 135-146 (2020).
[19] X. Cao, M. Jahazi, Mater. Des. **32**(1), 1-11 (2011).
[20] Y. Huang, L. Wan, X. Si, T. Huang, X. Meng, Y. Xie, Metall. Mater. Trans. A **50**, 295-299 (2019).

[21] Q. Song, Z. Ren, S. Ji, S. Niu, W. Qi, M. Chen, Adv. Eng. Mater. 1900973 (2019).
[22] Y. Wei, S.M. Rajiv, Magnesium technology Springer, Cham. p205-p209 (2011).
[23] S. Ren, Y.F. Bai, J. Chen, S.Z. Deng, N.S. Xu, Q.B. Wu, Mater. Lett. **61** (3), 666-670 (2007).
[24] L. Zhou, M.R. Yu, B.Y. Liu, Z.L. Zhang, S.W. Liu, X.G. Song, H.Y. Zhao, J. Mater. Res. Technol. **9** (1), 212-221 (2020).
[25] S. Ji, X. Meng, Z. Liu, R. Huang, Z. Li, Mater. Lett. **201**, 173-176 (2017).
[26] G. Song, L. Liu, P. Wang, Mat. Sci. Eng. A **429** (1-2), 312-319 (2006).
[27] N. Mahathaninwong, T. Plookphol, J. Wannasin, S. Visutmethangoon, Mat. Sci. Eng. A **532**, 91-99 (2012).
[28] Y.K. Yang, H. Dong, S. Kou, Weld. J. **87** (8), 202s-211s (2008).
[29] L.H. Shah, N.H. Othman, A. Gerlich, Sci. Technol. Weld. Joining. **23** (3), 256-270 (2018).
[30] B. Chen, Y. Wang, C. Xiao, M. Zhang, G. Ni, D. Li, Mater. Sci. Tech-Lond. **34** (6), 703-711 (2018).
[31] L. Ma, S.Y. Niu, S.D. Ji, P. Gong, Arch. Metall. Mater. **65** (1), 307-314 (2020).
[32] X. Gu, C. Sui, J. Liu, D. Li, Z. Meng, K. Zhu, Mater. Des. **181**, 108103 (2019).